

Nanoscale

Accepted Manuscript



This is an *Accepted Manuscript*, which has been through the Royal Society of Chemistry peer review process and has been accepted for publication.

Accepted Manuscripts are published online shortly after acceptance, before technical editing, formatting and proof reading. Using this free service, authors can make their results available to the community, in citable form, before we publish the edited article. We will replace this *Accepted Manuscript* with the edited and formatted *Advance Article* as soon as it is available.

You can find more information about *Accepted Manuscripts* in the [Information for Authors](#).

Please note that technical editing may introduce minor changes to the text and/or graphics, which may alter content. The journal's standard [Terms & Conditions](#) and the [Ethical guidelines](#) still apply. In no event shall the Royal Society of Chemistry be held responsible for any errors or omissions in this *Accepted Manuscript* or any consequences arising from the use of any information it contains.

Electroactive Biomimetic Collagen-Silver Nanowire Composite Scaffolds

Abeni Wickham,^a Mikhail Vagin,^b Hazem Khalaf,^c Sergio Bertazzo,^d Peter Hodder,^e Staffan Dånmark,^a Torbjörn Bengtsson,^c Jordi Altimiras,^f Daniel Aili^{a,*}

^aDivision of Molecular Physics, Department of Physics, Chemistry and Biology (IFM), Linköping University, SE-581 83 Linköping, Sweden, ^bDivision of Chemical and Optical Sensor Systems, Department of Physics, Chemistry and Biology (IFM), Linköping University, SE-581 83 Linköping, Sweden. ^cFaculty of Medicine and Health, School of Health and Medical Sciences, Örebro University, SE-701 82 Örebro, Sweden, ^dDepartment of Medical Physics and Biomedical Engineering, University College London, Malet Place Engineering Building, London, WC1E 6BT, UK, ^eTA Instruments Ltd. 730-740 Centennial Court, Centennial Way, Elstree WD6 3SZ, UK, ^fDivision of Biology, Department of Physics, Chemistry and Biology (IFM), Linköping University, SE-581 83 Linköping, Sweden.

*Email: daniel.aili@liu.se

Keywords: collagen, bioelectrodes, silver nanowires, charge storage, charge injection, embryonic cardiomyocytes

Abstract

Electroactive biomaterials are widely explored as bioelectrodes and as scaffolds for neural and cardiac regeneration. Most electrodes and conductive scaffolds for tissue regeneration are based on synthetic materials that have limited biocompatibility and often display large discrepancies in mechanical properties with the surrounding tissue causing problems during tissue integration and regeneration. This work shows the development of a biomimetic nanocomposite material prepared from self-assembled collagen fibrils and silver nanowires (AgNW). Despite consisting of mostly type I collagen fibrils, the homogeneously embedded AgNWs provide these materials with a charge storage capacity of about 2.3 mC cm^{-2} and a charge injection capacity of 0.3 mC cm^{-2} , which is on par with bioelectrodes used in the clinic. The mechanical properties of the materials are similar to soft tissues with a dynamic elastic modulus within the lower kPa range. The nanocomposites also support proliferation of embryonic cardiomyocytes while inhibiting the growth of both Gram-negative *Escherichia coli* and Gram-positive *Staphylococcus epidermidis*. The developed collagen/AgNW composites thus represent a highly attractive bioelectrode and scaffold material for a wide range of biomedical applications.

1. Introduction

Electroactive materials that can perform *in vivo* are central for numerous clinical applications, for example as electrodes used in neural prostheses, deep brain stimulation, and cardiac pacemakers. Various electrically active materials that can stimulate cellular electrotaxis and promote electrical coupling between cells have also been explored as tissue engineering (TE) scaffolds for wound healing,¹ regeneration of nerve tissue,² and cardiac regeneration.^{3,4,5} Although conventional materials for implantable electrodes, such as platinum, iridium, titanium nitride and iridium oxide,⁶⁻⁸ can provide high charge injection densities they are difficult to process into porous and degradable TE scaffolds. Therefore conjugated polymers have been widely examined. Polymers with high charge storage capacities, such as poly(3,4-ethylenedioxythiophene) (PEDOT), polypyrrole and polyaniline are, however, brittle and non-biodegradable,^{9,10} which can result in poor performance and potential complications in the host tissue.^{11,12} Incorporation of inorganic nanoparticles and nanowires into hydrogels have been explored as alternative strategies to make conductive materials that display mechanical and structural properties that are more similar to soft tissues.¹³ Metal nanoparticles embedded in biomimetic scaffolds have been shown to impart phenotypic traits in cultured cardiomyocytes that can improve the function of engineered cardiac tissue, without the need for exogenous electric stimulation.^{14,15} Cardiomyocytes cultured on hydrogels impregnated with conductive gold nanoparticle (AuNP) were shown to increase the connexin 43 (Cx43) expression, both with and without electrical stimulation, as compared to materials without AuNPs.¹⁴ A similar observation was made by Kohane et al. revealing that cardiomyocytes cultured on alginate scaffolds with clusters of gold nanowires (AuNWs) enhanced Cx43 expression without stimulation. The presence of AuNWs led to a significant increase in the amount of Cx43 and α -sarcomeric actinin as compared to when cultured on pristine alginate scaffolds.¹⁵ Moreover, silicon field effect transistors have also been introduced in hydrogels to

enable real time monitoring of electrochemical signals from cardiomyocytes and neural cells,¹⁶ and recently, polymer scaffolds supported by a magnesium foil were shown to be effective bioresorbable sensors for use in rat brains.¹⁷ Most of these materials, however ingenious, require complicated fabrication procedures and the use of materials that are not yet approved or suitable as medical implants.

Collagen is one of the main structural components of the extracellular matrices,¹⁸ and clinically, has been widely used in various biomaterial applications, such as bone fillers, wound dressings, and heart patches.¹⁹⁻²¹ Collagen in different forms can be found from the cornea to bones, where it is usually associated with other structural proteins and glycosaminoglycans. In some tissues, collagen interacts with inorganic components, e.g. in bone, where collagen fibril growth is initiated and oriented by hydroxyapatite nanoparticles.²² *In vitro*, collagen folding, self-assembly, and fibril formation can be mimicked using reconstituted collagen molecules in dilute acidic conditions.^{23,24} When the pH of the collagen solution is increased within a high salt environment, it initiates nucleation of the molecules.²⁵ Fibril growth rapidly commences once the solution is heated to 37°C. Plastic compression of collagen utilizes fibril reassembly to make tissue-like constructs mimicking the *in vivo* extracellular matrix (ECM).^{26,27} Albeit, an attractive biomaterial, collagen on its own is not conductive, and consequently has not been employed in bioelectronic applications. The introduction of conductive components to a collagen matrix would, however, allow for a biomimetic material that could improve stimulation, regeneration, and remodeling of tissues relying on electrical stimulation.

Silver nanowires (AgNWs) embedded in polydimethylsiloxane have been previously shown to result in highly conductive and stretchable materials.^{28,29} Silver nanomaterials have the added benefit of being a broad-spectrum antimicrobial agent, and are extensively used in

coatings for medical devices, and in wound care products.³⁰⁻³² Bacterial infections from implants are of considerable concern for the host as they lead to implant failure, chronic infections and subsequently can have dire effects on the patient quality of health.^{33,34} To obviate the risks of implant infections, various modifications to biomaterials with silver and silver nanoparticles (AgNPs) have been proposed.³⁵⁻³⁸ The toxicity of AgNPs to bacteria and other cells has been thoroughly investigated and is mainly an effect of the release of silver ions (Ag^+).³⁹ Concentration dependence of AgNP (< 80 nm) toxicity in suspension has been investigated for cell specific uptake into a range of different cell types, including mesenchymal stem cells, and embryonic neural stem cells, showing decreased metabolic activity at concentrations around 5 - 20 $\mu\text{g/ml}$.^{40,41} The toxicity is not directly dependent on the shape, size and geometry of the NPs, but the release rate of Ag^+ can be affected by NP surface to volume ratio and capping agents.⁴²⁻⁴⁴ AgNWs were found to be less toxic than AgNPs, and capping agents such as polyvinylpyrrolidone (PVP) or collagen further improve biocompatibility of the AgNWs without reducing the antimicrobial effects.⁴⁵⁻⁴⁷ The trapping of the AgNPs in a biocompatible matrix has been shown to reduce the *in vitro* and *in vivo* toxicity dramatically,^{48,49} presumably as a result of the slower release of Ag^+ .

Encouraged by these findings and with the ambition to develop an easily translatable, biomimetic, electroactive nanocomposite with the added functionality of sustained antimicrobial properties, we have developed a novel strategy for incorporation of AgNWs into fibrous collagen matrices. The resulting materials show AgNWs homogeneously incorporated in a native-like fibrillar collagen matrix. The nanocomposites demonstrate excellent charge injection and charge storage capacities, while retaining mechanical properties similar to soft tissues. The materials also supported the proliferation of embryonic chicken cardiomyocytes and showed antimicrobial activity against both Gram-negative and Gram-positive bacteria. The developed collagen/AgNW composite is a multifaceted material with electrical properties

comparable to metallic and conjugated polymer systems, with the added functionalities of tissue mimetic collagen composition, nanostructure and mechanical properties, and hence an interesting option for novel bioelectrodes and electroactive tissue regenerating scaffolds.

2. Experimental Section

Preparation of collagen/AgNW nanocomposites: A modified plastic compression procedure based on the technique developed by Brown et al. was used.⁵⁰ Briefly, lyophilized, rat-tail collagen (First Link, UK) was dissolved in 0.1 mM acetic acid at a concentration of 5 mg/ml. Minimum essential medium, MEM (First Link, UK) was added to the solution in a dilution of 1:10, MEM:collagen. The pH was then incrementally raised from 2 to 7 with 5 N NaOH. The solution was kept on ice for 10 minutes before the addition of different concentrations of silver nanowires (0.1-5 mg/ml final concentration) with an average diameter 90 nm and length 30 μm , dissolved in water (Blue Nano, USA). The suspensions were then incubated for 20 minutes at 37°C, before being compressed between 200 μm spaced nylon and stainless steel meshes. The materials were kept in 1X phosphate buffered saline for storage.

Scanning electron microscopy (SEM) and Energy-dispersive X-ray spectroscopy (EDS): Samples were dried using increasing concentrations of ethanol in water and finally in hexamethyldisilazane (HMDS) for 15 minutes. These samples were then sputter coated with a 10 nm layer of platinum (Leica EM SCD 500) and then imaged at an accelerating voltage of 5 kV (Leo 1550 Gemini, Zeiss, Germany). EDS was carried out using 80 mm² X-Max Silicon Drift Detector and the AztecEnergy software (Oxford Instruments). The elemental analysis were collected in the form of a map together with the electron microscopy image and spectra, with an accelerating voltage of 20 kV and working distance of 8.5 mm for all samples.

Density-dependent colour scanning electron microscopy (DDC-SEM) imaging was performed with the composites attached to a sample holder, which was then coated with a 10 nm layer of chromium (Quorum Technologies Sputter Coater model K575X). The nanocomposites were imaged by SEM (Gemini 1525 FEGSEM), operating at 10 kV. The DDC-SEM images were obtained by imaging a region in backscatter mode and subsequently imaging the same region in the in-lens mode. With the ImageJ software, images were stacked and the in-lens image was assigned to the green channel, whereas the backscatter image was assigned to the red channel.

Inductively coupled plasma-optical emission spectroscopy (ICP-OES): The concentration of silver ions was measured with ICP-OES Optima 8000 (PerkinElmer). The samples were dried and dissolved with a nitric acid/hydrochloric acid solution over night. The samples were then diluted and compared to the Ag standard curve at 338 nm.

Electrochemical characterization: Screen-printed graphite disk electrodes (SPE), diameter 1.8 mm, were obtained from Rusens LTD (Moscow, Russia). Collagen/AgNW nanocomposites were made with the electrodes incorporated during incubation at 37°C and then compressed as mentioned above. An Autolab type III potentiostat (Autolab, EcoChemie, Netherlands) was employed for voltammetric and amperometric measurements. A saturated calomel electrode (SCE) (Radiometer, Copenhagen) and a platinum wire were used as the reference electrode and counter electrode, respectively. The Anson equation (eq. 1) was utilized for the analysis of chronocoulometry data:

$$Q = nFAC\sqrt{\frac{Dt}{\pi}} \quad (1)$$

where Q is the charge (C), n the number of electrons transferred in single reaction, F the Faraday constant (96487 C mol⁻¹), A the surface area (cm²), C the concentration of substance

undergoing electrode process (M), D the diffusion coefficient ($\text{cm}^2 \text{s}^{-1}$) and t the time (s). Electrochemical impedance spectroscopy (EIS) was carried out in a 10 mM potassium ferricyanide and 10 mM potassium ferrocyanide 0.1 M KCl solution at an applied potential of 0.22 V (versus Ag/AgCl) from 0.1 to 105 Hz with a voltage amplitude of 10 mV.

Rheology: Rheological properties of the nanocomposites were investigated using the TA Instruments Discovery Hybrid Rheometer DHR-3, an 8 mm stainless steel parallel plate and standard Peltier plate as the temperature module, controlling the temperature isothermally at 37°C. Tests were performed in an immersion cell with the sample immersed in phosphate buffered saline, pH 7.4. A small controlled axial force was used to provide a slight positive loading pressure on the samples to ensure good contact.

Cell isolation and proliferation assays: Fertilized Ross 308 broiler chicken eggs were obtained from a hatchery (Lantmännen Swehatch, Väderstad, Sweden) and incubated at 37.8°C, with a relative humidity of 45% and 21% oxygen, for 19 days. Isolation of cardiomyocytes was done with approval from the Linköping Ethical Committee (Dnr. 9-13) following procedures previously described.⁵¹ Briefly, embryonic chicken cardiomyocytes (ECCM) were harvested after collecting whole hearts into Tyrode's buffer (pH 7.35, 5 mM KCl, 10 mM glucose, 140 mM NaCl, 1 mM MgCl₂, 10 mM HEPES) kept at 4°C. The atria were cleaved and removed. The ventricles were minced and exposed to enzymatic degradation with 120 U/ml collagenase and 0.525 U/ml protease for 10 minutes at 37°C. The supernatant of the enzymatic solution was collected up to 10 repeats and centrifuged for 5 minutes at 300 g. The pellet was suspended in Tyrode's buffer supplemented with 200 μM Ca²⁺ and kept on ice. The aliquots were then pooled, centrifuged and the pellets resuspended in Tyrode's with 400 μM Ca²⁺. The cells were pre-plated in cell culture media with 1 mM Ca²⁺ for 1.5 h to remove endothelial cells and fibroblasts and enrich the cardiomyocyte

fraction. ECCMs remaining in suspension were then centrifuged, resuspended, counted, plated in cell culture flasks and kept in a cell incubator at 37°C, 5% CO₂ for two days before seeding on the collagen/AgNW nanocomposite materials. The materials were cut with a 6 mm trephine to fit into the wells of 96 well plates and cleaned overnight in 3X penicillin/streptomycin in sterile PBS at 4°C. Just before cell seeding the wells were rinsed thrice with PBS. The ECCMs were seeded at a density of 10⁴ cell/well in supplemented DMEM (10% FBS, 1% Essential Amino Acids, 1% Sodium Pyruvate and 1% penicillin/streptomycin). The cells were grown on the materials for up to 7 days, and the media exchanged every other day. Cell proliferation rates were tested using the 3-(4,5-dimethylthiazol-2-yl)-5-(3-carboxymethoxyphenyl)-2-(4-sulfophenyl)-2H-tetrazolium, inner salt (MTS) assay (CellTiter96[®] Aqueous one solution, Promega, Madison, WI) following the instructions provided by the manufacturer. First, the materials were placed into new wells and the media was changed to starvation DMEM (with 0 % FBS) before adding 20 µL of MTS reagent and the absorbance was read at 490 nm (ASYS UVM240 microplate reader). At the same time intervals, a Live/Dead assay was performed by using Live/Dead[®] Viability/Cytotoxicity Kit (Life Technologies, CA, USA). The materials were imaged at each time point with a confocal fluorescence microscope (Zeiss LSM 700). SEM imaging was done on samples at the same time points using the protocol explained in a previous section.

Antimicrobial evaluation: *Escherichia coli* MG1655 and *Staphylococcus epidermidis* were grown on Luria-Bertani (LB)-agar plates overnight at 37°C. Single colonies were inoculated into 5 ml LB broth and the tubes were incubated at 37°C overnight on shaker set at 200 rpm. The bacterial suspension was inoculated into 5 ml LB broth or spread (100 µl) onto LB-agar plates. The nanocomposites were cut into 6 mm diameter pieces and placed into the tubes and onto the LB plates. Bacterial growth was monitored over time by measuring the optical

density at 620 nm (Multiskan Ascent, Thermo Labsystems) and by microscopically studying the colony density (Olympus CKX41 microscope coupled with Olympus SC30 camera).

Statistical analysis: Statistical analysis on MTS results was done using multiple comparisons two-way ANOVA, post hoc Tukey's test, with GraphPad Prism (La Jolla CA, USA). Statistical significance was assigned at $p < 0.05$ and are indicated with an asterisk (*). In some instances p values < 0.0001 were calculated and are indicated with (****). P values > 0.05 were denoted as not significant and labeled as 'ns'.

3. Results and Discussion

3.1 Materials Synthesis and Characterization

Extracellular matrix (ECM) mimetic collagen materials were prepared by plastic compression of rat-tail type I collagen at a concentration of 5 mg/ml, which resulted in well-defined collagen fibrils that assembled into a fibrous matrix (Fig. 1). Collagen fibril formation was initiated by raising the pH of collagen dissolved in dilute acetic acid to pH 7. After gelation at 37°C, a mechanical load was applied while allowing controlled release of water from the collagen gel using capillary flow into a filter.

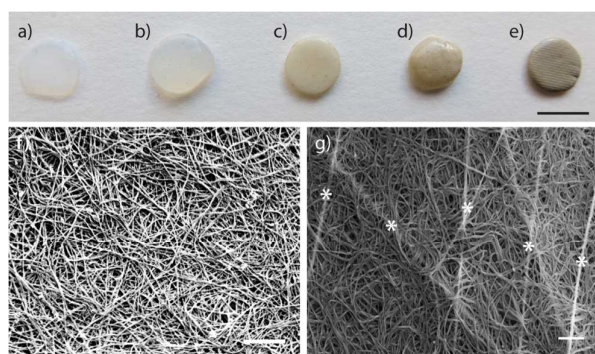


Fig. 1 Optical images of a) Control, 0 mg/ml, b) 0.1 mg/ml, c) 0.5 mg/ml, d) 1 mg/ml, and e) 5 mg/ml collagen/AgNW nanocomposites. Scale bar: 6 mm. Scanning electron microscopy (SEM) images of f) Control, 0 mg/ml, and g) 1 mg/ml collagen/AgNW nanocomposite, * indicates AgNWs. Scale bars: 1 μ m.

Collagen/AgNW nanocomposites were obtained by introducing AgNWs to the collagen solution just after the nucleation of collagen fibrils, i.e. after increasing the pH to 7. Samples were made with 0.1, 0.5, 1 and 5 mg/ml AgNWs with respect to the initial collagen solution volume (Fig. 1). The resulting nanocomposite materials had a distinctive silver appearance at the highest AgNW concentrations after compression (Fig. 1c-e). The dimensions of the

AgNWs used here were on average 90 nm in diameter and 30 μm in length (Fig. S1†), which is similar to the size of the collagen fibers (Fig. 1 f, g and Fig. S2†). The addition of nanowires during collagen fibril formation assured formation of scaffolds with homogeneously dispersed nanowires, ensconced within the collagen matrix. Additionally, the length of the AgNWs facilitated formation of a conductive network even when the NWs were significantly diluted in the collagen matrix. SEM imaging did not reveal any significant differences in collagen fibril morphology or appearance of the compressed collagen network after addition of AgNWs (Fig. S2†). Density dependent coloring (DDC) in conjunction with SEM enabled the distinction between the AgNWs (yellow) and the collagen fibrils (green) in Fig. 2. Increasing the concentrations of AgNWs resulted in a denser network of NWs in the nanocomposites but without formation of any visible aggregates.

Electron dispersive X-ray spectroscopy (EDS) was utilized to confirm the presence and distribution of AgNWs in the compressed collagen. The EDS spectra (Fig. S3†) show large comparative increases of Ag with the increasing concentrations of Ag, as expected with the exception of the sample prepared using 0.1 mg/ml AgNWs, which only showed a marginal increase from the control indicated by the presence of Ag L α 1 in the EDS spectrum (Fig. S3†, inset).

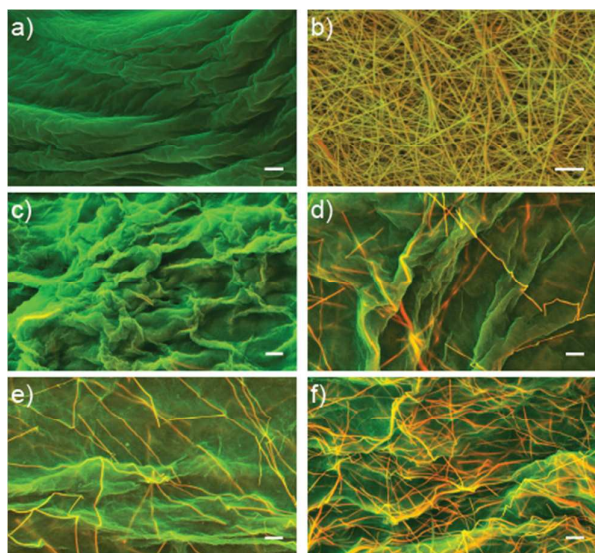


Fig. 2 DDC-SEM micrographs of a) collagen after plastic compression (green), b) AgNWs (yellow), and collagen/AgNWs nanocomposites prepared using c) 0.1 mg/ml, d) 0.5 mg/ml, e) 1 mg/ml, f) 5 mg/ml AgNWs. Scale bars: 2 μm .

3.2 Electrochemical properties

The dried collagen/AgNW nanocomposites with 5 mg/ml of AgNWs showed a sheet resistance of 600-500 Ω/cm^2 , clearly indicating that the NWs form a continuous conducting network. The nanocomposites with lower concentrations of AgNWs showed significantly higher sheet resistance values that could not be measured properly with a four-point probe. Since the ability to inject and store charges in the wet state are the most important property of electroactive scaffold materials, the electrochemical properties of the nanocomposites were evaluated by inserting a screen-printed graphite disk electrodes into the collagen/AgNW suspension before the onset of the gelation, i.e. before incubation at 37°C, and then compressed to form the nanocomposites. Electrochemical impedance spectroscopy (EIS) measurements in PBS revealed a decrease in double layer capacitance (Fig. S4†) of the

nanocomposites as compared to the pure collagen as estimated from the geometrical circle fit of the impedance spectra in complex capacitive coordinates. The EIS measurements in faradaic processing conditions using ferro/ferricyanide as a redox probe, revealed a non-monotonous change in the electrode reaction rate with the presence of AgNWs (Fig. 3a). The two time-resolved processes representing the whole impedance response observed in the Bode plot (Fig. 3a) can be represented as two resistor-capacitor (RC) elements in the unified equivalent circuit (Fig 3a, Inset) utilized for fitting the spectra. This simplest equivalent circuit consisted of a solution resistance (R_S) in series with two charge transfer resistances (R_{CT}). In order to represent the electrode surface inhomogeneity, a constant phase element (CPE) was introduced instead of a pure capacitance. The capacitance values were calculated as (eq. 2):

$$C_{DL} = (R_S(P)^{(1-\phi)})^{1/\phi} \quad (2)$$

where R_S is a solution resistance, P and ϕ are the fitting parameters of the CPE⁵². Similarly to the double layer capacitance, the capacitances estimated for the two aforementioned processes decreased in the presence of AgNWs (Fig. 3a). The resistances, which are inversely proportional to the process rates, showed a distinguishably different behavior with increasing concentration of AgNWs (Fig. 3b-c). Representing the slower process (I), the larger resistance revealed a minor dependence on the AgNW concentration, whereas the faster process (II) showed smaller resistance and a significant increase in the rate with increasing concentration of AgNWs. The slow process (I) represents the ionic conductivity through the film, while the concentration dependent fast process (II) represents the electronic conductivity through the film. The increase in AgNW concentration lead only to the electronic conductivity increase, while the ionic conductivity remained largely unaffected.

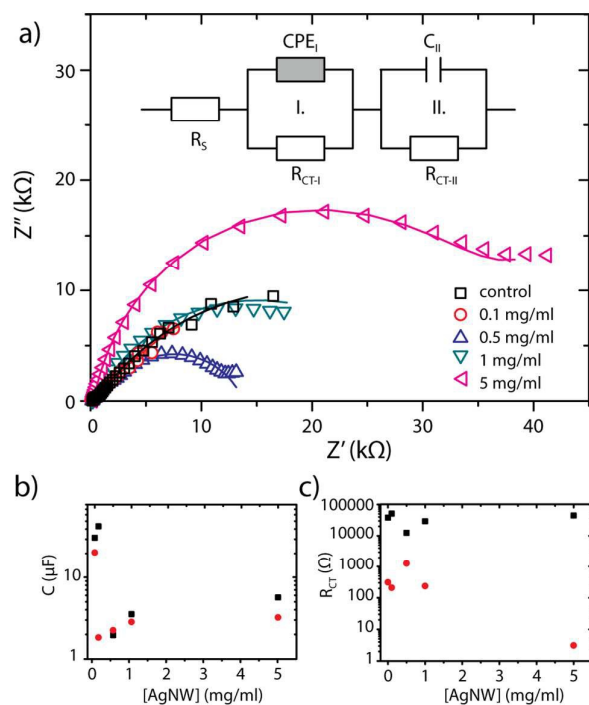


Fig. 3 a) Impedance spectra in Nyquist coordinates of the collagen/AgNW nanocomposites in 10 mM ferro/ferricyanide solution in PBS at 0.2 V. Solid lines: fitted curves. Inset: unified equivalent circuit. b) The dependence of capacitances, and c) charge transfer resistances on the AgNW concentration. Black squares and red circles represent processes I and II, respectively.

Cyclic voltammetry (CV) showed capacitive currents at both cathodic and anodic regions that varied non-linearly with the concentration of AgNWs (Fig. S5†). However, the contributions of Ag redox reactions could not be readily resolved with this technique. Presumably because the AgNWs are both capped with polyvinylpyrrolidone (PVP) and embedded in the dense collagen matrix.

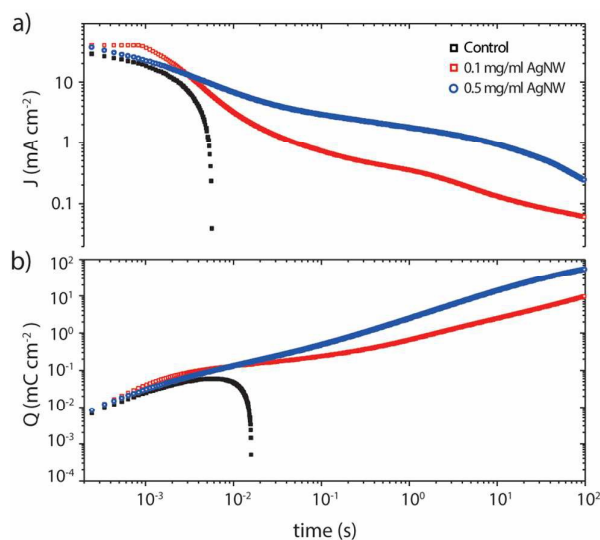


Fig. 4 Charge injection properties of collagen, 0.1 and 0.5 mg/ml collagen/AgNW nanocomposites. The transients of a) current and, b) charge densities, obtained at 0.6 V pulse with pure collagen (black squares) and collagen/AgNW composites (0.1 mg/ml (red squares) and 0.5 mg/ml (blue circles) AgNW).

The faradaic charge storage capacity of the nanocomposites was investigated using chronoamperometry in a wide domain of sampling times. The measurements were carried out under conditions suitable for cell stimulation using the inherent redox-activity of the embedded AgNW, i.e. no additional redox active species were added. A long potential pulse from the regions of low (0 V) to high currents (0.6 V) was applied to the materials. The recorded transient current densities showed a significant change in the characteristics for the nanocomposites as compared to the collagen only materials (Fig. 4a and Fig. S6†). The pure collagen samples (0 mg/ml AgNWs) showed lower currents with a fast decay whilst the 0.1, and 0.5 mg/ml collagen/AgNW nanocomposites revealed dramatically slower decays of currents characterized by slopes close to -0.5 in double logarithmic coordinates. This

illustrates the Cottrell's current decay due to the influence of the electrode reaction by planar diffusion, where the increase in AgNW concentration led to higher currents.

Transients of surface-normalized integral charge (Fig. 4b) showed that the collagen/AgNW nanocomposites have a charge storage capacity that increased with time, reaching values of 2.3 mC cm^{-2} and 12.3 mC cm^{-2} at the 10 s pulse for AgNW concentrations of 0.1 mg/ml and 0.5 mg/ml, respectively. As a comparison, the charge storage capacity of optimized electrode materials for neural stimulation are for iridium oxide, 28.8 mC cm^{-2} ,⁸ polypyrrole, 48.8 mC cm^{-2} ,⁵³ poly(3,4 ethylenedioxythiophene), 75.6 mC cm^{-2} ,^{54,55} whereas platinum electrodes in pacemakers show a charge storage capacity of $208 \text{ } \mu\text{C cm}^{-2}$.⁵⁶ The charge injection capacity, i.e. the amount of charges that can move through the electrodes, characterized at shorter times, reached a value of 0.33 mC cm^{-2} and 0.94 mC cm^{-2} at a pulse time of 300 ms for 0.1 mg/ml and 0.5 mg/ml collagen/AgNW, respectively. This is about the same order of magnitude as the charge injection capacity reported for polypyrrole-based neural electrodes (1.17 mC cm^{-2}) developed for electrical stimulation of skeletal muscles.⁵³

The Anson plot was used for the linearization of the obtained charge transients (Fig. S7†). Assuming the concentration of substance undergoing electrode process is equal to metallic silver, one can calculate the apparent diffusion coefficients of Ag^+ ions inside the collagen composites: $1 \times 10^{-10} \text{ cm}^2 \text{ s}^{-1}$ and $0.7 \times 10^{-10} \text{ cm}^2 \text{ s}^{-1}$ for the 0.1 mg/ml and 0.5 mg/ml collagen/AgNW nanocomposites, respectively. These values are small enough to illustrate the efficient entrapment of the AgNWs within the collagen matrix.

3.3 Mechanical properties

Rheology was used to explore the influence of AgNWs on the dynamic mechanical properties of the collagen fibers. Collagen will deform like a solid until there is a relaxation of the

deformation, where the fluid-like behaviors are indicative of molecular rearrangements.⁵⁷ The materials were immersed in PBS buffer (pH 7.4) at 37°C during the measurements, since dehydration of the collagen fibrils would significantly alter the mechanical properties of the nanocomposites.⁵⁸ Small differences in thickness and swelling characteristics of each sample were accounted for by applying a small controlled axial force to provide a slight positive pressure to the top of the sample, which ensured a good contact (Fig. S8†). A series of oscillatory experiments, and amplitude and frequency sweeps were used to investigate the frequency dependency of the viscoelastic properties of materials.

All samples showed frequency independence for a wide frequency range, suggesting hydrated network structures (Fig. S9†). The addition of AgNWs had a small effect on the storage modulus (G') of the materials, though; it did affect the loss modulus (G'') significantly (Fig. 5a). The nanocomposites with 0.5 mg/ml AgNWs showed higher G' values and lower G'' values than materials with 0.1 mg/ml AgNWs, and significantly lower G'' than collagen only matrices, suggesting that the AgNWs contributed to the increased rigidity of the material. With increasing torques there was a significant increase in G'' in samples with 0.5 mg/ml AgNWs, indicating that the interactions between AgNWs and collagen fibers were disrupted resulting in the more fluid-like behavior.

A step transient creep test was performed to investigate creep ringing of the material, which shows differences in rigidity and fiber network associations (Fig. 5b). Materials with 0.5 mg/ml AgNWs showed lower amplitudes and dampened faster than the pure collagen (control), whereas materials with 0.1 mg/ml AgNWs showed the opposite. The AgNWs consequently seem to disrupt the collagen network and at the lowest concentration (0.1 mg/ml) of AgNWs, the NWs were too dispersed to reinforce the material. In the materials with 0.5 mg/ml AgNWs, on the other hand, the density of the AgNWs was high enough to

reinforce the collagen network. This was further confirmed by the higher G' and lower G'' values for nanocomposites with 0.5 mg/ml AgNWs as compared to materials with 0.1 mg/ml AgNWs (Fig. 5a).

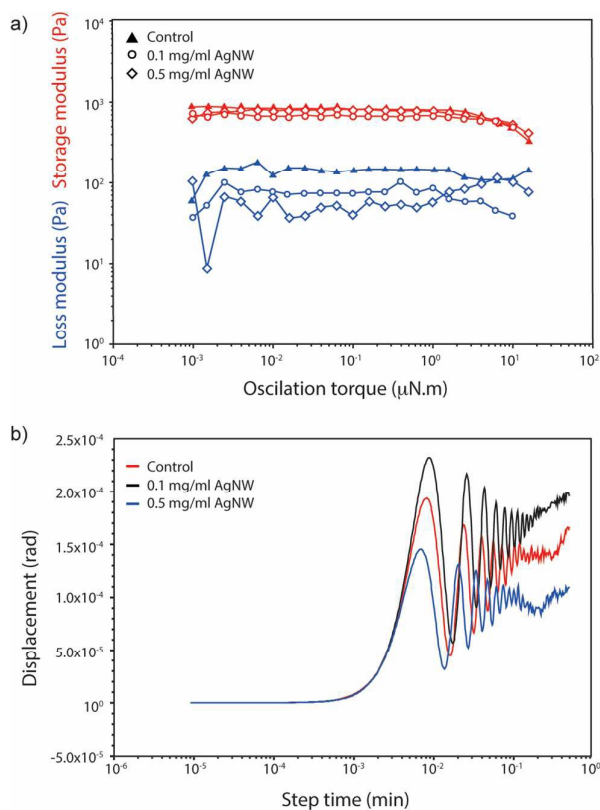


Fig. 5 a) Amplitude sweeps showing the storage modulus (G') and loss modulus (G''), and b) step transient creep ringing of collagen matrices and collagen/AgNW nanocomposites with 0 (control), 0.1 and 0.5 mg/ml AgNWs.

Soft gels with a modulus around 1 kPa have been shown to efficiently support and produce beating cardiomyocytes,⁵⁹ and these nanocomposites are in the same range. In addition, the relatively high concentration of collagen (5 mg/ml) used for the preparation of the

collagen/AgNW nanocomposites allows for a more sturdy material apt for suturing as compared to the much softer collagen matrices resulting from lower collagen concentrations normally used (2-3 mg/ml).^{60,61}

3.4 Cytocompatibility

Cell adhesion and proliferation are determining factors for the concentration of AgNWs that can be used in a clinical setting. As an initial evaluation of the effect of AgNW concentrations on cell proliferation, we carried out Live/Dead Cytotoxicity and MTS colorimetric proliferation assays of embryonic chicken cardiomyocytes (ECCMs) cultured on the developed collagen/AgNW nanocomposites. SEM images were acquired at the same time points to further characterize cell morphology. Freshly isolated ECCM were chosen as a suitable model as they are very sensitive to both the mechanical and morphological properties of scaffold materials.^{62,63}

The cells were seeded on the nanocomposites with a density of 10^4 cells/well, where the bottom of each well was covered by a circular piece of the matrix. Cell proliferation was tracked for seven days. The presence of AgNWs affected the proliferation rate of the cells after day 5, where the samples with the highest concentrations (0.5 and 1 mg/ml) showed reduced proliferation rates as compared to the collagen control (0 mg/mL AgNWs) (Fig. 6a). When normalized to the day 7 controls, all samples retained a similar proliferation capacity up to day 5, with the exception that the proliferation was significantly higher on samples with 0.1 mg/ml compared to the control at day 3, $p < 0.05$. At the highest AgNW concentration (0.5 and 1 mg/ml), proliferation peaked at day 5, and by day 7 there were significantly fewer cells than on materials with 0.1 mg/ml AgNWs and the controls (Fig. 6a, $p < 0.001$). There was no significant difference at day 7 between either the control and 0.1 mg/ml or between the 0.5 mg/ml and 1 mg/ml concentrations. The Live/Dead assay showed a similar trend (Fig. 6b).

There were hardly any dead cells, noted by the lack of red emission of the ethidium homodimer-1, while there was a similar emission of green from the hydrolyzed calcein acetomethoxy, i.e., living cells on the control and 0.1 mg/ml materials.

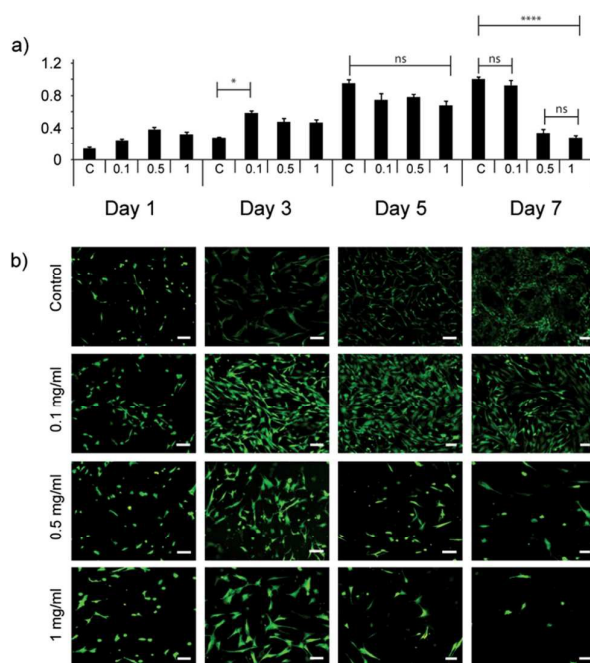


Fig. 6 a) MTS assay showing the proliferation of embryonic cardiomyocytes on nanocomposites with different concentrations of AgNWs from Day 1 to 7. The data is normalized with respect to the day 7 collagen control samples. There was a significant lag in growth on the control sample at day 3 ($p < 0.05$). By day 5, all samples had no statistically significant difference, but on day 7 the 0.5 and 1 mg/ml significantly dropped in cell numbers ($p < 0.0001$). The 0.1 mg/ml samples were not statistically significantly different from the control samples in the cell proliferation on day 7. b) Live/Dead imaging of ECCMs on nanocomposites with different concentrations of AgNWs. Notice the absence of red staining indicative of dead cells. Scale bars: 10 μm .

This lack of imaged dead cells could be due to the combined effect of high local concentrations of Ag^+ and the presence of polyvinylpyrrolidone (PVP) on the AgNW. PVP is used to promote the anisotropic growth of the silver into AgNWs and also supports their colloidal stability.⁶⁴ Although PVP has been shown to increase biocompatibility of silver nanowires for alveolar epithelial cells,⁶⁵ PVP is also known to hinder cell adhesion.⁶⁶ Proliferation of cardiomyocytes depends on their proximity to each other, as their survival is reliant on the formation of interconnected networks formed at higher seeding densities.⁶⁷ As some cells detached after day 5, there was not a sufficient cell density to promote proliferation on the higher concentrations of collagen/AgNW nanocomposites, seen in the day 7 overview images of the material (Fig. S10†). This is further confirmed in the SEM images where the cells are rounded and detaching from the areas with high concentrations of AgNWs (Fig. 7).

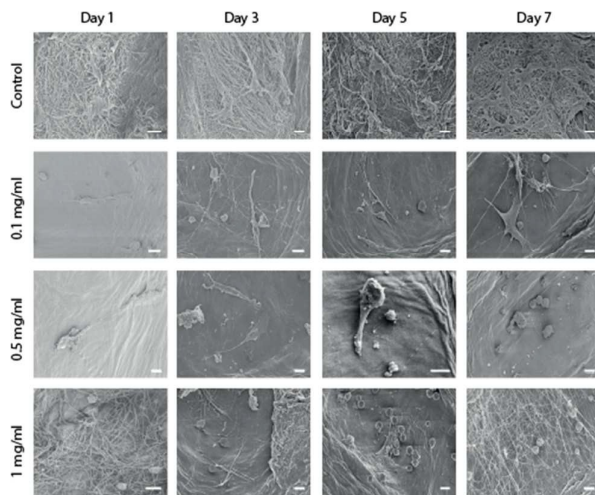


Fig. 7 Scanning electron microscopy of embryonic cardiomyocytes cells on control (collagen and 0 mg/ml AgNWs) and collagen/AgNW nanocomposites. Increasing concentrations of AgNWs resulted in rounded and detached cells. The 0, 0.1, and 0.5 mg/ml AgNW samples showed cells with extended morphologies indicative of adhesion. Scale bar: 10 μm

Protrusions of filopodia were seen on the collagen control as well as on nanocomposites with 0.1. The cells on the 0.5 mg/ml samples showed extended morphologies, up until day 5. Rounded cells were found where there were locally high densities of AgNWs (Fig. 6). The lowest concentration of AgNW (0.1 mg/ml) showed no significant difference in cell proliferation as compared to the pure collagen control. Despite showing both very high charge storage and injection capacities, the actual concentration of silver in the nanocomposite was just about 2.6 ppm as determined using inductively coupled plasma-optical emission spectroscopy (ICP-OES). This concentration is well below the 10 ppm, which tend to show negative effects on immune cell populations,⁶⁸ and below the >20 ppm used for water treatments, for example.⁶⁹

3.5 Antimicrobial Properties

Silver (Ag) has been used for many decades as a powerful antimicrobial agent in hospital settings,⁷⁰ and has been used to treat and prevent infections at least since the 1920s.⁷¹ Numerous studies have shown the use of AgNP coatings on catheters and other biomaterials to be effective against infections.^{72,73} The bactericidal effects of Ag⁺ is thought to be an effect of direct damage to the cell membranes, disruption of ATP production and DNA replication, and generation of reactive oxygen species (ROS).⁷⁴ The antimicrobial effect of AgNWs or AgNPs in any form has been shown to be indirectly a result of the release of silver ions (Ag⁺).³⁹

The antimicrobial effects of the collagen/AgNW nanocomposite were investigated against Gram-negative *Escherichia coli* and Gram-positive *Staphylococcus epidermidis* bacteria using the standard agar plate test and broth assay. For both bacterial strains, growth inhibition only occurred at the surfaces of the nanocomposites and not in suspension. No inhibition of bacterial growth was seen in solution using the broth assay as expected because of the limited

leakage of Ag^+ from the materials in combination with dilution of the released ions (Fig. S11†). Materials with AgNWs were found to suppress the growth of *E.coli* and *S.epidermidis* (Fig. 8) on Luria-Bertani (LB) plates, as indicated by the zones of inhibition. The growth on LB plates was completely suppressed by surfaces containing the highest concentrations of AgNWs (1 and 5 mg/ml). The concentration of AgNWs supporting proliferation of cardiomyocytes (0.1 mg/ml) also showed a zone of inhibition dictating localized antimicrobial activity. Furthermore, the materials without AgNWs were almost completely covered by bacterial colonies after 72 hours (Fig. 8). Inhibition of bacterial growth on the surface of implants and bioelectrodes is of large importance, as secondary bacterial infection can cause severe complications and even trigger implant rejection.⁷⁵ The nanocomposites with the lowest AgNW concentrations thus offer both localized inhibition of both *E.coli* and *S.epidermidis* while retaining the same proliferation capacity for cardiomyocytes as a collagen only matrix.

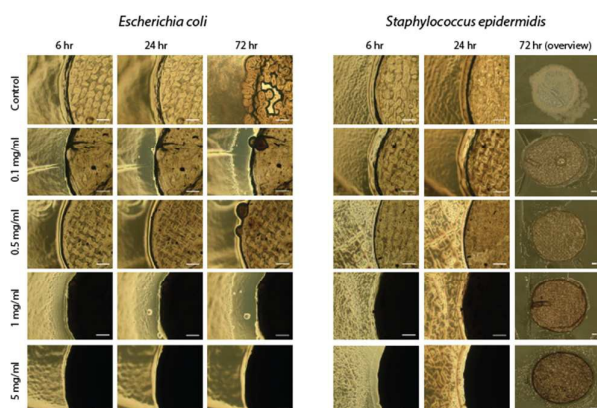


Fig. 8 Antimicrobial activity of the nanocomposites against *E.coli* and *S.epidermidis* assessed by agar disc diffusion method over 6 - 72 hours. The inhibition of bacterial growth on or near the nanocomposites improved with increasing concentration of AgNWs. Scale bars: 500 μm .

4. Conclusions

Here we show the development of collagen/silver nanowire (AgNW) nanocomposites that are simple to fabricate and offer multiple functionalities, in addition to mimicry of the multi-scale structural complexity of the extracellular matrix. The nanocomposites mainly consist of fibrillar collagen and behave as soft gels with a storage modulus of about 1 kPa, but display charge storage and injection capacities in the similar range as notable electrode materials like platinum and iridium oxide. Electrical impedance spectroscopy showed that the addition of AgNWs significantly increases the electronic conductivity, while having marginal effect on the ionic conductivity. The lowest concentration of AgNW (0.1 mg/ml during synthesis and 2.6 ppm Ag in the final sample) showed no significant difference in proliferation of freshly isolated embryonic cardiac cell as compared to the collagen control, whereas higher concentrations of AgNWs led to a reduction in cell numbers and proliferation after seven days of culture. The antimicrobial properties provided by the AgNWs also simplify handling and storage of the materials while reducing need for antibiotics in a potential clinical application. The materials described here, present a new approach to fabricate soft tissue mimetic bioelectrodes and scaffolds for tissue engineering applications benefitting from efficient electrical stimulation.

Acknowledgements

D.A., A.W., and J.A. gratefully acknowledge financial support from Linköping University and the Swedish Foundation for Strategic Research (SSF). During this study, A.W. was enrolled in the graduate school Forum Scientium. We would like to thank Fatemeh Ajallouelian, Hanna Österman, Amy Gelmi, Fredrik Björefors for helpful discussions. We would also like to thank Jeannette Steffen and Matthew Harrington for help with ICP-OES experiments.

† Electronic Supplementary Information (ESI) available: See DOI:10.1039/x0xx00000x

References

- 1 L. C. Kloth, *Int. J. Low. Extrem. Wounds*, 2005, **4**, 23.
- 2 A. Fabbro, A. Sucapane, F. M. Toma, E. Calura, L. Rizzetto, C. Carrieri, P. Roncaglia, V. Martinelli, D. Scaini, L. Masten, A. Turco, S. Gustincich, M. Prato and L. Ballerini, *PLoS ONE*, 2013, **8**, e73621.
- 3 W.-H. Zimmermann, I. Melnychenko, G. Wasmeier, M. Didié, H. Naito, U. Nixdorff, A. Hess, L. Budinsky, K. Brune, B. Michaelis, S. Dhein, A. Schwoerer, H. Ehmke and T. Eschenhagen, *Nat. Med.*, 2006, **12**, 452.
- 4 N. Tandon, C. Cannizzaro, P.-H. G. Chao, R. Maidhof, A. Marsano, H. T. H. Au, M. Radisic and G. Vunjak-Novakovic, *Nat. Protoc.*, 2009, **4**, 155.
- 5 G. Vunjak-Novakovic, K. O. Lui, N. Tandon and K. R. Chien, *Annu. Rev. Biomed. Eng.*, 2011, **13**, 245.
- 6 L. A. Geddes and R. Roeder, *Ann. Biomed. Eng.*, 2003, **31**, 879.
- 7 S. F. Cogan, P. R. Troyk, J. Ehrlich and T. D. Plante, *IEEE Trans. Biomed. Eng.*, 2005, **52**, 1612.
- 8 S. F. Cogan, *Annu. Rev. Biomed. Eng.*, 2008, **10**, 275.
- 9 R. A. Green, N. H. Lovell, G. G. Wallace and L. A. Poole-Warren, *Biomaterials*, 2008, **29**, 3393.
- 10 R. Balint, N. J. Cassidy and S. H. Cartmell, *Acta Biomater.*, 2014, **10**, 2341.
- 11 J. P. Harris, J. R. Capadona, R. H. Miller, B. C. Healy, K. Shanmuganathan, S. J. Rowan, C. Weder and D. J. Tyler, *J. Neural Eng.*, 2011, **8**, 066011.
- 12 I. R. Mineev, P. Musienko, A. Hirsch, Q. Barraud and N. Wenger, *Science*, 2015, **347**, 159.

- 13 P. Schexnaider and G. Schmidt, *Colloid Polym. Sci.*, 2008, **287**, 1.
- 14 J.-O. You, M. Rafat, G. J. C. Ye and D. T. Auguste, *Nano Lett.*, 2011, **11**, 3643.
- 15 T. Dvir, B. P. Timko, M. D. Brigham, S. R. Naik, S. S. Karajanagi, O. Levy, H. Jin, K. K. Parker, R. Langer and D. S. Kohane, *Nat. Nanotech.*, 2011, **6**, 720.
- 16 B. Tian, J. Liu, T. Dvir, L. Jin, J. H. Tsui, Q. Qing, Z. Suo, R. Langer, D. S. Kohane and C. M. Lieber, *Nat. Mat.*, 2012, **11**, 1.
- 17 S.-K. Kang, R. K. J. Murphy, S.-W. Hwang, S. M. Lee, D. V. Harburg, N. A. Krueger, J. Shin, P. Gamble, H. Cheng, S. Yu, Z. Liu, J. G. McCall, M. Stephen, H. Ying, J. Kim, G. Park, R. C. Webb, C. H. Lee, S. Chung, D. S. Wie, A. D. Gujar, B. Vemulapalli, A. H. Kim, K.-M. Lee, J. Cheng, Y. Huang, S. H. Lee, P. V. Braun, W. Z. Ray and J. A. Rogers, *Nature*, 2016, DOI: 10.1038/nature16492.
- 18 M. D. Shoulders and R. T. Raines, *Annu. Rev. Biochem.*, 2009, **78**, 929.
- 19 W. Friess, *Euro. J. Pharm. Biopharm.*, 1998, **45**, 113.
- 20 L. Cen, W. Liu, L. Cui, W. Zhang and Y. Cao, *Pediatr. Res.*, 2008, **63**, 492.
- 21 E. S. Place, N. D. Evans and M. M. Stevens, *Nat. Mat.*, 2009, **8**, 457.
- 22 Y. Wang, T. Azaïs, M. Robin, A. Vallée, C. Catania, P. Legriel, G. Pehau-Arnaudet, F. Babonneau, M.-M. Giraud-Guille and N. Nassif, *Nat. Mat.*, 2012, **11**, 724.
- 23 D. J. S. Hulmes, *J. Struct. Biol.* 2002, **137**, 2.
- 24 K. Kadler, D. Holmes, J. Trotter and J. Chapman, *Biochem. J.*, 1996, **316**.
- 25 M. Yan, B. Li, X. Zhao and S. Qin, *Food Hydrocolloids*, 2012, **29**, 199.
- 26 U. Cheema and R. A. Brown, *Adv. Wound Care*, 2013, **2**, 176–184.
- 27 H. J. Levis, G. S. L. Peh, K.-P. Toh, R. Poh, A. J. Shortt, R. A. L. Drake, J. S. Mehta and J. T. Daniels, *PLoS ONE*, 2012, **7**, e50993.
- 28 F. Xu and Y. Zhu, *Adv. Mater.*, 2012, **24**, 5117.
- 29 G.-S. Liu, C. Liu, H.-J. Chen, W. Cao, J.-S. Qiu, H.-P. D. Shieh and B.-R. Yang, *Nanoscale*, 2016, DOI: 10.1039/c5nr06237c.

- 30 K. K. Y. Wong and X. Liu, *Med. Chem. Commun.*, 2010, **1**, 125.
- 31 J. A. Lemire, J. J. Harrison and R. J. Turner, *Nat. Med.*, 2013, **11**, 371.
- 32 D. J. Barillo and D. E. Marx, *Burns*, 2014, **40**, S3.
- 33 J. M. Schierholz and J. Beuth, *J. Hosp. Infec.*, 2001, **49**, 87.
- 34 R. O. Darouiche, *N. Engl. J. Med.*, 2004, **350**, 1422.
- 35 Y. Barnea, J. Weiss and E. Gur, *Ther. Clin. Risk Manage.*, 2010, **6**, 21.
- 36 M. L. W. Knetsch and L. H. Koole, *Polymers*, 2011, **3**, 340.
- 37 V. S. Cardoso, P. V. Quelemes, A. Amorin, F. L. Primo, G. G. Gobo, A. C. Tedesco, A. C. Mafud, Y. P. Mascarenhas, J. R. C. a, S. A. Kuckelhaus, C. Eiras, J. R. S. Leite, D. Silva and J. R. dos Santos Junior, *J. Nanobiotechnol*, 2014, **12**, 36.
- 38 V. Q. Nguyen, M. Ishihara, J. Kinoda, H. Hattori, S. Nakamura, T. Ono, Y. Miyahira and T. Matsui, *J. Nanobiotechnol*, 2014, **12**, 49.
- 39 Z.-M. Xiu, Q.-B. Zhang, H. L. Puppala, V. L. Colvin and P. J. J. Alvarez, *Nano Lett.*, 2012, **12**, 4271.
- 40 C. Greulich, J. Diendorf, T. Simon, G. Eggeler, M. Epple and M. Köller, *Acta Biomater.*, 2011, **7**, 347.
- 41 F. Liu, M. Mahmood, Y. Xu, F. Watanabe, A. S. Biris, D. K. Hansen, A. Inselman, D. Casciano, T. A. Patterson, M. G. Paule, W. Slikker and C. Wang, *Front. Neurosci.*, 2015, **9**, 1.
- 42 R. Kumar and H. Münstedt, *Biomaterials*, 2005, **26**, 2081.
- 43 J. Liu and R. H. Hurt, *Environ. Sci. Technol.*, 2010, **44**, 2169.
- 44 L. Pauksch, S. Hartmann, M. Rohnke, G. Szalay, V. Alt, R. Schnettler and K. S. Lips, *Acta Biomater.*, 2014, **10**, 439.
- 45 M. Rai, A. Yadav and A. Gade, *Biotechnol. Adv.*, 2009, **27**, 76.
- 46 C. Marambio-Jones and E. M. V. Hoek, *J. Nanopart. Res.*, 2010, **12**, 1531.
- 47 E. I. Alarcon, K. Udekwu, M. Skog, N. L. Pacioni, K. G. Stampelcoskie, M. González-

- Béjar, N. Poliseti, A. Wickham, A. Richter-Dahlfors, M. Griffith and J. C. Scaiano, *Biomaterials*, 2020, **33**, 4947.
- 48 H. Wang, M. Cheng, J. Hu, C. Wang, S. Xu and C. C. Han, *ACS Appl. Mater. Interfaces*, 2013, **5**, 11014.
- 49 C.-H. Chen, S.-H. Chen, K. T. Shalumon and J.-P. Chen, *Acta Biomater.*, 2015, **26**, 225.
- 50 R. A. Brown, M. Wiseman, C. B. Chuo, U. Cheema and S. N. Nazhat, *Adv. Funct. Mater.*, 2005, **15**, 1762.
- 51 A. C. B. Svensson Holm, I. Lindgren, H. Osterman and J. Altimiras, *Physiol. Rep.*, 2014, **2**, e12182.
- 52 V. D. Jovic and B. M. Jovic, *J. Electroanal. Chem.*, 2003, **541**, 1.
- 53 L. Guo, M. Ma, N. Zhang, R. Langer and D. G. Anderson, *Adv. Mater.*, 2014, **26**, 1427.
- 54 S. J. Wilks, S. M. Richardson-Burns, J. L. Hendricks, D. C. Martin and K. J. Otto, *Front. Neuroeng.*, 2009, **2**, 1–8.
- 55 S. Venkatraman, J. Hendricks, Z. A. King, A. J. Sereno, S. Richardson-Burns, D. Martin and J. M. Carmena, *IEEE Trans. Neural Syst. Rehabil. Eng.*, 2011, **19**, 307–316.
- 56 A. Norlin, J. Pan and C. Leygraf, *J. Electrochem. Soc.*, 2005, **152**, J7.
- 57 M. Shayegan and N. R. Forde, *PLoS ONE*, 2013, **8**, e70590.
- 58 A. Masic, L. Bertinetti, R. Schuetz, S.-W. Chang, T. H. Metzger, M. J. Buehler and P. Fratzl, *Nat. Commun.*, 2015, **6**, 1.
- 59 A. J. Engler, C. Carag-Krieger, C. P. Johnson, M. Raab, H. Y. Tang, D. W. Speicher, J. W. Sanger, J. M. Sanger and D. E. Discher, *J. Cell Sci.*, 2008, **121**, 3794.
- 60 H. J. Levis, R. A. Brown and J. T. Daniels, *Biomaterials*, 2010, **31**, 7726.
- 61 C. E. Ghezzi, N. Muja, B. Marelli and S. N. Nazhat, *Biomaterials*, 2011, **32**, 4761.
- 62 M. A. Laflamme, J. Gold, C. Xu, M. Hassanipour, E. Rosler, S. Police, V. Muskheli and C. E. Murry, *Am. J Pathol.*, 2010, **167**, 663.
- 63 L. R. Madden, D. J. Mortisen, E. M. Sussman, S. K. Dupras, J. A. Fugate, J. L. Cuy, K.

- D. Hauch, M. A. Laflamme, C. E. Murry and B. D. Ratner, *Proc. Natl. Acad. Sci.*, 2010, **107**, 15211.
- 64 Y. Sun, B. Mayers, T. Herricks and Y. Xia, *Nano Lett.*, 2003, **3**, 955.
- 65 L. C. Stoehr, E. Gonzalez, A. Stampfl, E. Casals, A. Duschl, V. Puentes and G. J. Oostingh, *Part. Fibre Toxicol.*, 2011, **8**, 36.
- 66 G. Gorfu, I. Virtanen, M. Hukkanen, V. P. Lehto, P. Rousselle, E. Kenne, L. Lindbom, R. Kramer, K. Tryggvason and M. Patarroyo, *J. Leukocyte Biol.*, 2008, **84**, 701.
- 67 W. A. Clark, M. L. Decker, M. Behnke-Barclay, D. M. Janes and R. S. Decker, *J. Mol. Cell. Cardiol.*, 1998, **30**, 139.
- 68 H.-J. Yen, S.-H. Hsu and C.-L. Tsai, *Small*, 2009, **5**, 1553.
- 69 N. L. Martin, P. Bass and S. N. Liss, *PLoS ONE*, 2015, **10**, e0131345.
- 70 P. L. Drake and K. J. Hazelwood, *Ann. Occup. Hyg.*, 2005, **49**, 575.
- 71 A. Kissmeyer, *Br. J. Vener. Dis.*, 1928, **4**, 199.
- 72 M. Fischer, M. Vahdatzadeh, R. Konradi, J. Friedrichs, M. F. Maitz, U. Freudenberg and C. Werner, *Biomaterials*, 2015, **56**, 198.
- 73 S. A. Brennan, C. Ni Fhoglu, B. M. Devitt, F. J. O'Mahony, D. Brabazon and A. Walsh, *Bone Joint J.*, 2015, **97B**, 582.
- 74 W.-R. Li, X.-B. Xie, Q.-S. Shi, H.-Y. Zeng, Y.-S. OU-Yang and Y.-B. Chen, *Appl. Microbiol. Biotechnol.*, 2009, **85**, 1115.
- 75 A. S. Chong and M.-L. Alegre, *Nat. Rev. Immunol.*, 2012, **12**, 459.